Electronic Supplementary Information

Enhanced visible light photocatalytic hydrogen production over poly(dibenzothiophene-S,S-dioxide)-based heterostructures decorated by earth-abundant layered double hydroxides

Jingsong Luo, Jun Wu, Yuxiang Liu, Jiahuan Yuan and Feng Wang*

School of Chemical Engineering and Pharmacy, Wuhan Institute of Technology, Wuhan 430205, P. R. China.

** Corresponding author. E-mail: psfwang@wit.edu.cn (F. Wang)*

Experimental section

Materials

All chemicals used in this work were purchased from Aladdin Reagent Co., Ltd. $Ni(NO_3)_2 \cdot 6H_2O$, $Fe(NO_3)_3 \cdot 9H_2O$, NaOH, Na_2CO_3, and $Pd(PPh_3)_4(0)$ were used as received without further purification.

Synthesis of NiFeLDH

NiFeLDH was synthesized using the coprecipitation method at room temperature with a molar ratio of Ni^{2+}/Fe^{3+} = 7. $Ni(NO_3)_2 \cdot 6H_2O$ (8.143 g, 0.028 mol/L) and $Fe(NO_3)_3 \cdot 9H_2O$ (1.616 g, 0.004 mol/L) were dissolved in 20 mL deionized water to obtain a metal salt solution. Then NaOH (1.5 mol/L, 5 mL) and Na_2CO_3 (0.015 mol/L, 10 mL) were added dropwise into the solution until pH = 9. The resulting slurry was stirred vigorously for 24 h at room temperature and then the precipitate formed was filtered and washed several times with distilled water to remove excess soluble ions until the pH of the filtrate reached 7. The washed precipitate was dried in an oven at 60 °C overnight and then it was crushed to powder form for further use.

Synthesis of PSO@NiFeLDH

The as-synthesized composites were named as PSO@NiFeLDH-X, where X stands for the feed mass ratio between dibenzothiophene-S,S-dioxide and NiFeLDH. The PSO@NiFeLDH-15 denotes dibenzothiophene-S, S-dioxide in the presence of

15% NiFeLDH. The following is a typical process for synthesizing PSO@NiFeLDH-15.

Under argon protection, 3,7-bis(4,4,5,5-tetramethyl-1,3,2-dioxaborolan-2-yl)dibenzothiophene-S,S-dioxide (234 mg, 0.5 mmol), 3,7-dibromodibenzothiophene-S,S-dioxide (187 mg, 0.5 mmol), $Pd(PPh_3)_4(0)$ (15 mg, 0.012 mmol), and NiFeLDH (23.8 mg) were added into a mixture of DMF (40 mL) and Na_2CO_3 (2 mol/L, 6 mL). The resulting mixture was heated to 150 °C with vigorous stirring for 72 h. The composite was recovered by filtration, continuous washed with distilled water and methanol, and ultimately dried overnight at 90 °C.

Photocatalytic activity evaluation

The photocatalysis test was conducted on a Labsolar-6A circulation system (Beijing Perfectlight Technology Co., Ltd). A Xe lamp (300 W) was used as a light source for photocatalysis ($\lambda > 420$ nm). Typically, 10 mg of photocatalyst was ultrasonically dispersed in 100 mL triethanolamine (TEOA) aqueous solution. The temperature was kept at 10 °C by flowing a cooling system for the test. The generated hydrogen was quantified using an online gas chromatograph (GC-7806, nitrogen carrier) equipped with a packed column and a flame ionization detector (FID) by the external standard method. The standard curve of hydrogen was exhibited in Fig. S20. The hydrogen sample generated by the photocatalytic reaction is fed into the Labsolar-6A all-glass automatic online gas analysis system, and the target gas is fed into the gas chromatography every hour to measure the amount of hydrogen produced through the all-glass online injection valve (Fig. S21).

Characterization

Solid state ^{13}C CP-MAS NMR analysis was performed to confirm the chemical structure of PSO by a 400 MHz Bruker Advance instrument at a MAS rate of 10 kHz. Elemental analyses (C, H, O, S) were recorded on an Elementar Vario EL cube elemental analyzer. Powder X-ray diffraction (XRD) analysis was carried out on an X-ray diffractometer Rigaku Smart Lab. The fourier transform infrared (FT-IR) spectroscopy was collected on KBr disks using a Bruker Tensor II FT-IR spectrometer in transmission mode. The nanomorphology of the polymers was observed by field-

emission scanning electron microscopy (SEM, HITACHI, JSM-7001F) and high-resolution transmission electron microscopy (HRTEM, HITACHI, H-7650). The binding energies determined by X-ray photo-electron spectroscopy (XPS, PHI-Vesoprobe 5000 Ш) were corrected by reference to the adventitious carbon peak (284.8 eV) for each sample. UV–vis diffuse reflectance spectra (UV–vis DRS) were recorded on a SHIMADZU UV-2600 spectrophotometer. Photoluminescence (PL) spectra were measured under excitation wavelength at 420 nm (Shimadzu, F-7000 PC). Time-resolved PL was acquired on an Edinburgh FLS980 spectrophotometer. The ultraviolet photo-electron spectroscopy (UPS) was measured on Thermo ESCALAB XI+. The electron paramagnetic resonance (EPR) was carried out on CIQTEK EPR200-Plus. The content of Ni and Fe in sample was measured by Inductively Coupled Plasma–Mass Spectrometry (ICP-MS, Agilent 7700s). Thermogravimetric analysis (TGA) was performed by using a thermal analysis instrument (SDT-Q600) and the samples were heated up to 700 °C at a rate of 10 °C min^{-1} under nitrogen atmosphere for each sample. The solid surface area were calculated from N_2 adsorption isotherms, measured at 77 K on QUADRASORB evo. The Barret-Joyner-Halenda (BJH) model was used to get Brunauer-Emmett-Teller (BET)-specific surface area and the average pore size.

Apparent quantum yield (AQY) measurement

The AQY measurement for the photocatalytic experiment was carried out using monochromatic Xe lamp (300 W) with band pass filter. The light intensities at 420, 450, and 500 nm are 29.1, 30.6, 39.2 mW cm^{-2}, respectively. During the photocatalysis, PSO@NiFeLDH-15 (10 mg) nanocomposite was suspended in 100 mL aqueous solution in the presence of TEOA (20 vol%). The AQY was calculated based on following equation:

$$AQY(\%) = \frac{2 \times Number\ of\ evolved\ H_2\ molecules}{Number\ of\ incident\ photons} \times 100\%$$

Electrochemical measurement

The electrochemical impedance spectroscopy (EIS) and cyclic voltammetry (CV) were measured for the photoelectrochemical properties using a CHI 600 electrochemical workstation (Shanghai, China). A three-electrode cell system was

immersed into electrolyte solution with Bu_4NPF_6 acetonitrile solution. The samples were prepared by the mixture slurry of polymer and 5 wt% Nafion. The resulting slurry was coated on a glass substrate and dried at 50 °C under vacuum before the measurement. A platinum plate and a saturated calomel electrode (SCE) as were used as the counter electrode and reference electrode, respectively. CV measurements were conducted at a scan rate of 50 mV/s under nitrogen atmosphere. The ferrocene/ferrocenium (Fc/Fc+) reference was used as an internal standard, which was assigned an absolute energy of −4.8 eV vs vacuum level. The lowest unoccupied molecular orbital (LUMO) energy levels and the highest occupied molecular orbital (HOMO) energy levels of polymers were calculated by the empirical formulas of $E_{HOMO} = -e(E_{ox} + 4.8 - E_{1/2}^{(Fc/Fc+)})$ (eV) and $E_{LUMO} = -e(E_{re} + 4.8 - E_{1/2}^{(Fc/Fc+)})$ (eV) respectively, where E_{re} and E_{ox} are the onset of the reduction and oxidation potential vs SCE.

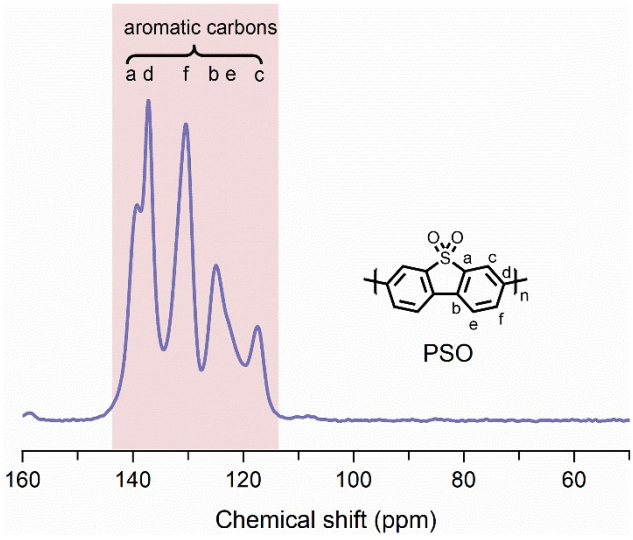

Fig. S1 Solid-state ^{13}C NMR spectra of PSO.

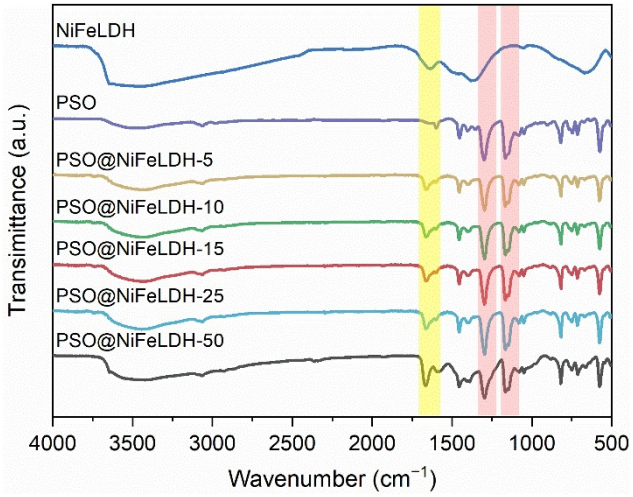

Fig. S2 FT-IR spectra of NiFeLDH, PSO and PSO@NiFeLDH composites.

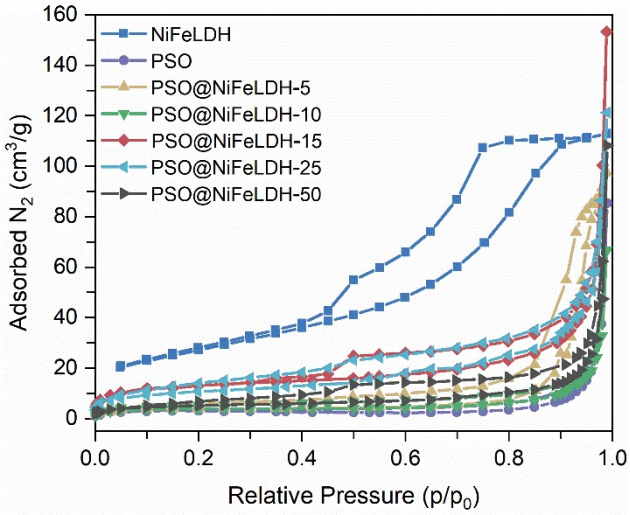

Fig. S3 Nitrogen adsorption-desorption isotherms of NiFeLDH, PSO and PSO@NiFeLDH composite.

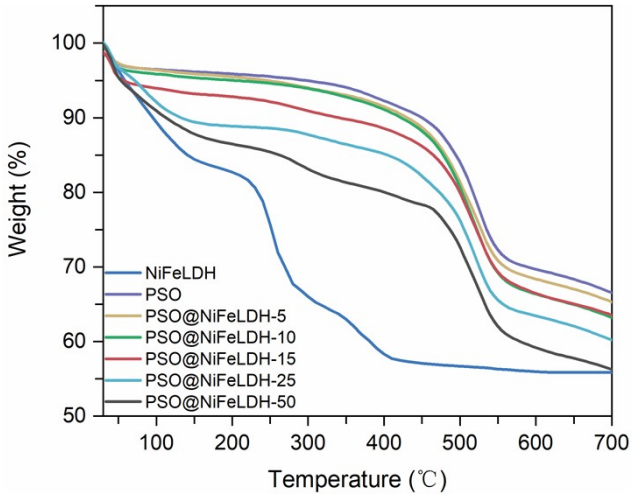

Fig. S4 TGA of NiFeLDH, PSO and PSO@NiFeLDH composite.

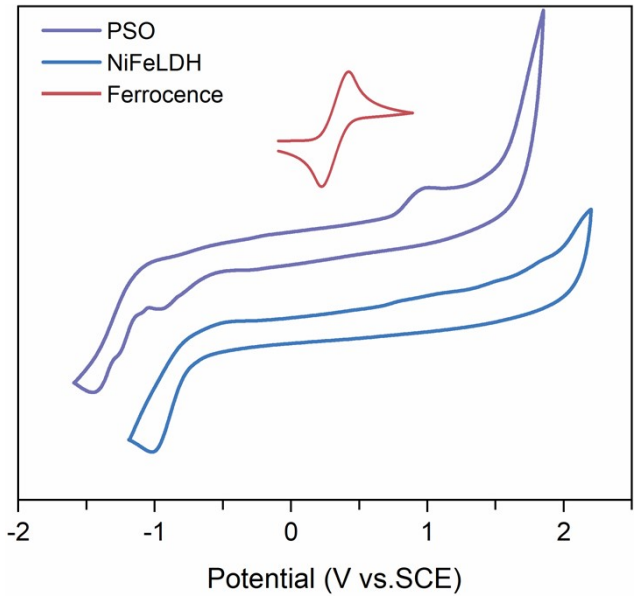

Fig. S5 CV curves of NiFeLDH and PSO.

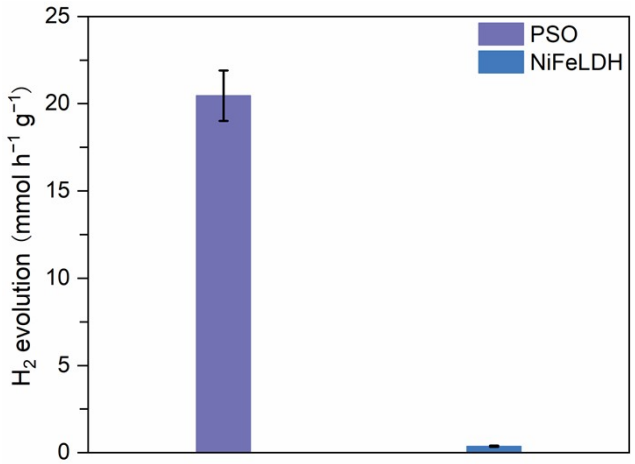

Fig. S6 The HERs of NiFeLDH and PSO with TEOA under visible light irradiation.

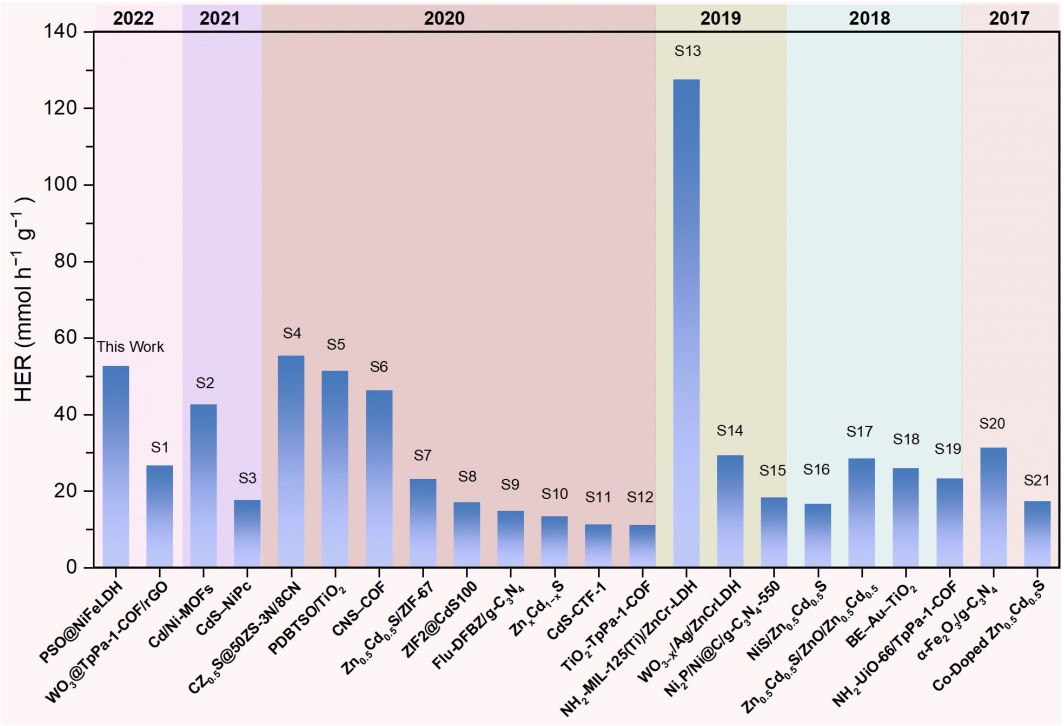

Fig. S7 The HER for PSO@NiFeLDH in comparison with representative heterojunction photocatalysts. (HER > 10 mmol h^{-1} g^{-1}). The concrete test details are described in Table S5.

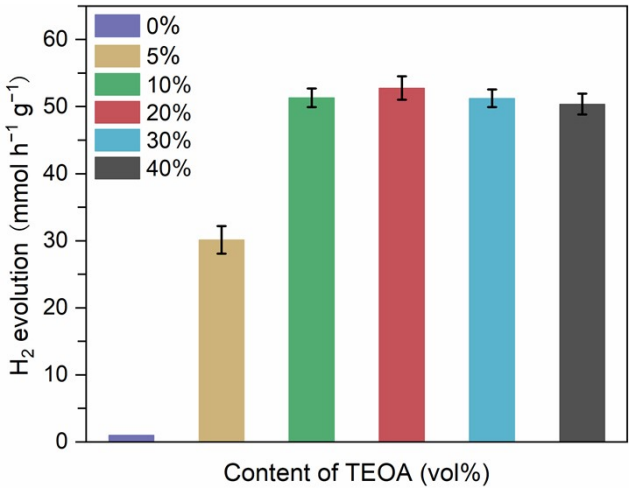

Fig. S8 The HERs of PSO@NiFeLDH-15 with different concentration of TEOA under visible light irradiation.

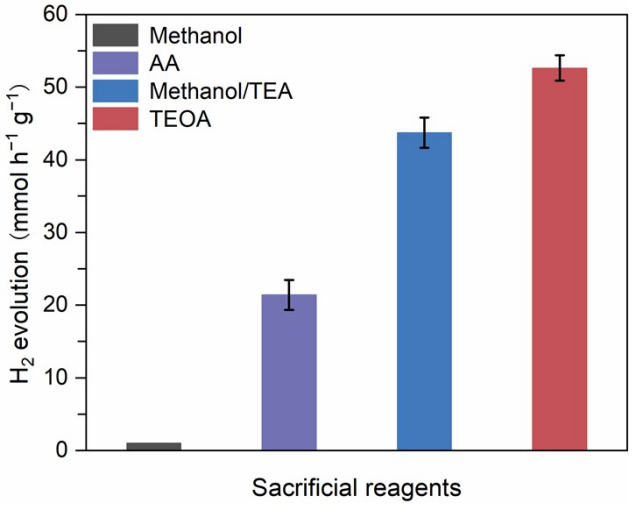

Fig. S9 The HERs of PSO@NiFeLDH-15 with different sacrificial agent under visible light irradiation.

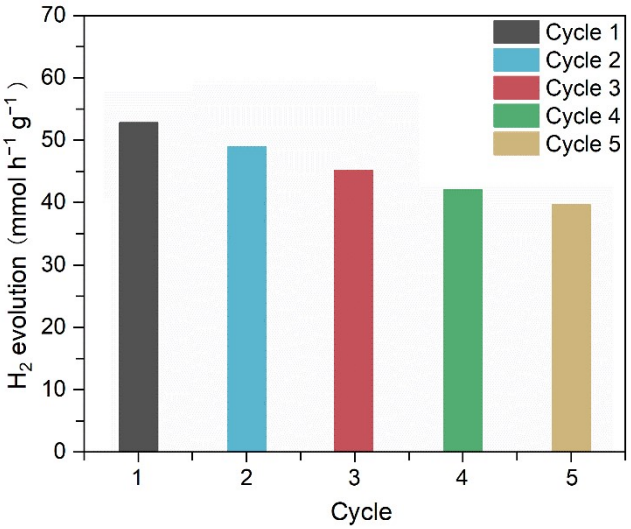

Fig. S10 The HERs of PSO@NiFeLDH-15 composite for each cycle of stability test.

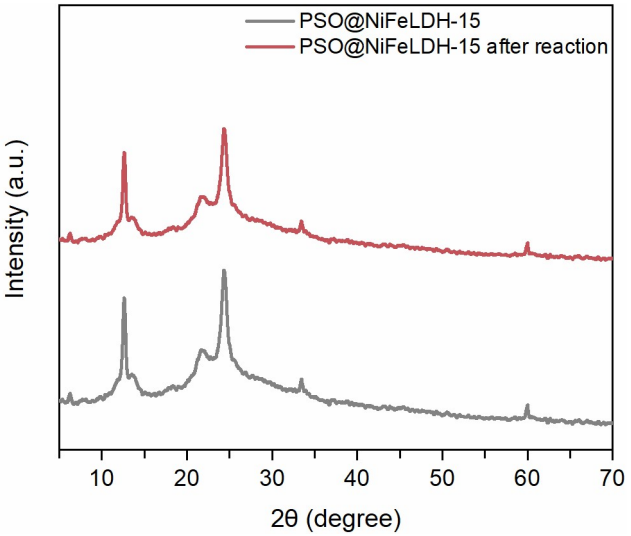

Fig. S11 XRD patterns of PSO@NiFeLDH-15 before and after the photocatalytic reaction.

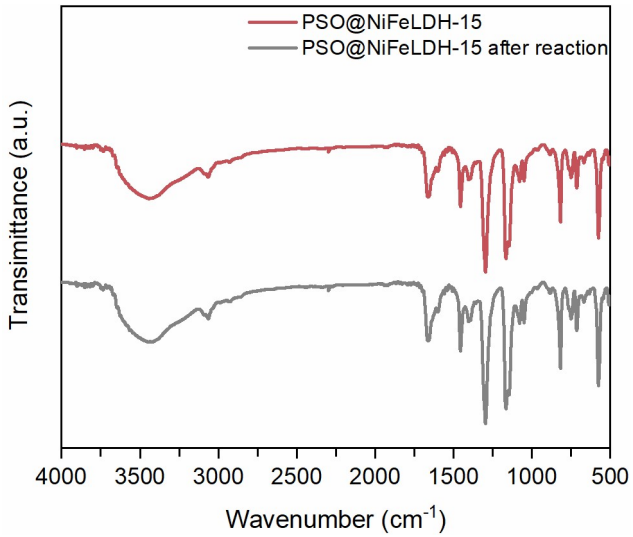

Fig. S12 FT-IR spectra of PSO@NiFeLDH-15 before and after the photocatalytic reaction.

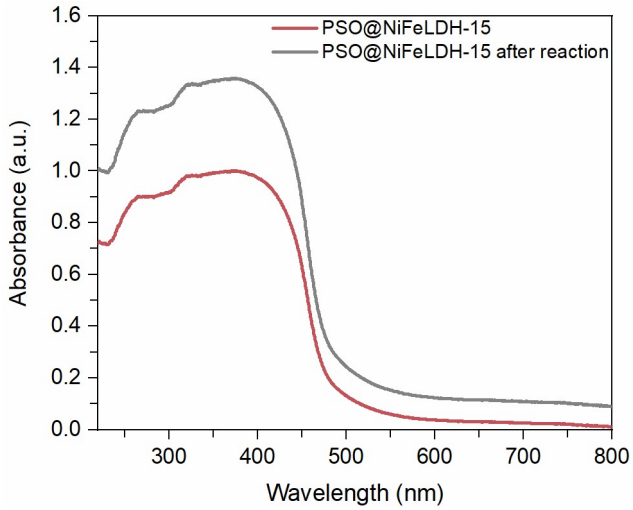

Fig. S13 UV–vis DRS of PSO@NiFeLDH-15 before and after the photocatalytic reaction.

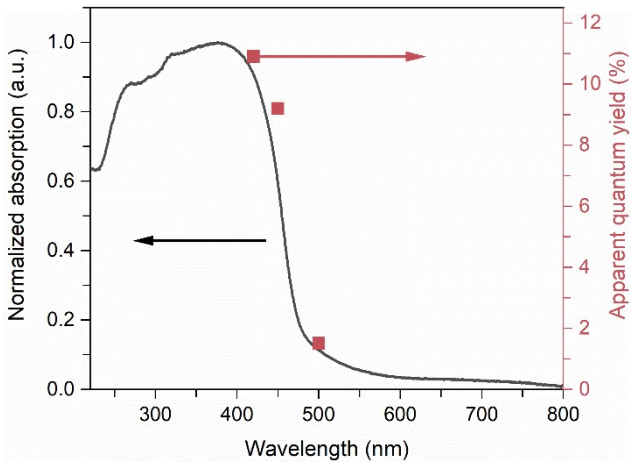

Fig. S14 Wavelength dependence of AQY on hydrogen production and UV-vis absorption spectra of PSO@NiFeLDH-15.

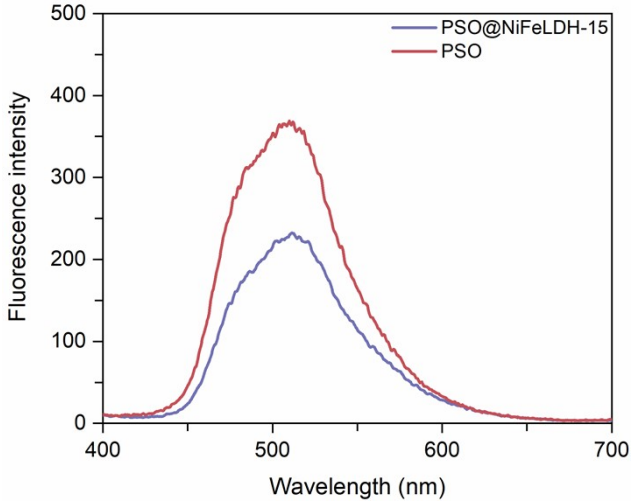

Fig. S15 PL spectra of PSO and PSO@NiFeLDH-15.

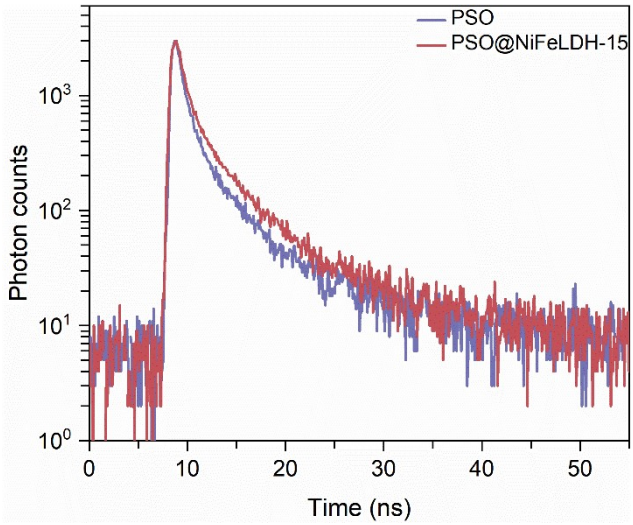

Fig. S16 Time-resolved PL spectra of PSO and PSO@NiFeLDH-15.

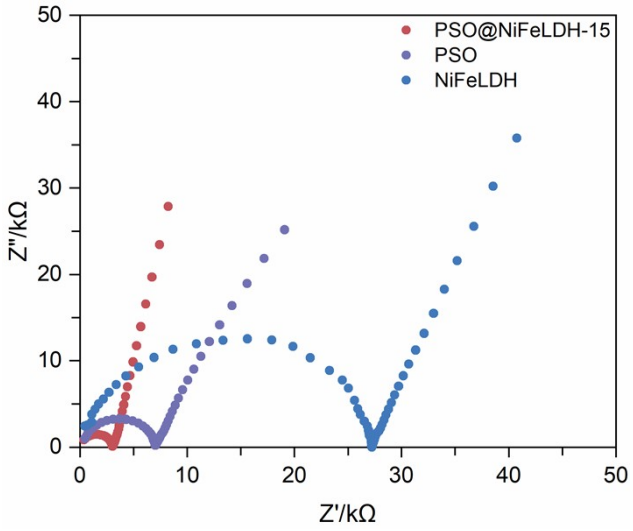

Fig. S17 EIS spectroscopy of NiFeLDH, PSO and PSO@NiFeLDH-15.

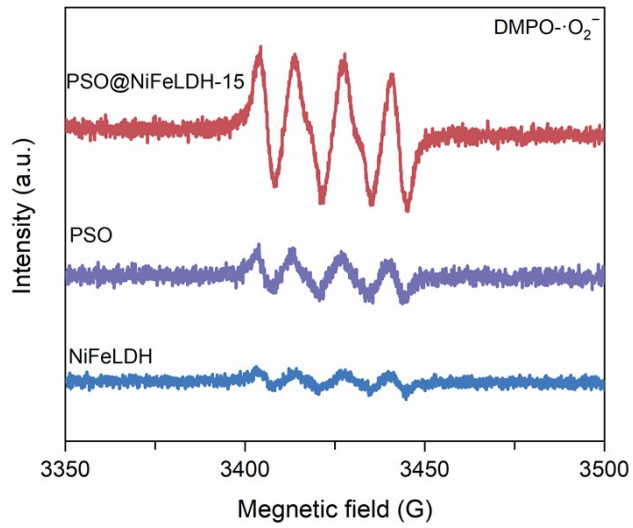

Fig. S18 EPR spectra of DMPO-·O_2^- for NiFeLDH, PSO and PSO@NiFeLDH-15 composite with DMPO as free radical trapping agent.

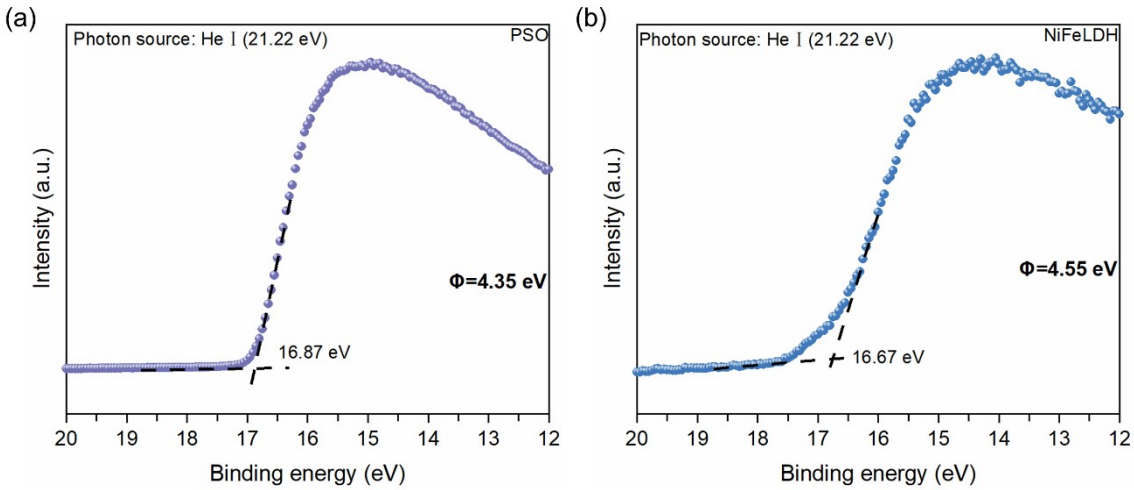

$\Phi = h\nu - E_{SE}$, where E_{SE} is secondary edges, $h\nu$=21.22 eV.

Fig. S19 UPS spectra of (a) PSO and (b) NiFeLDH.

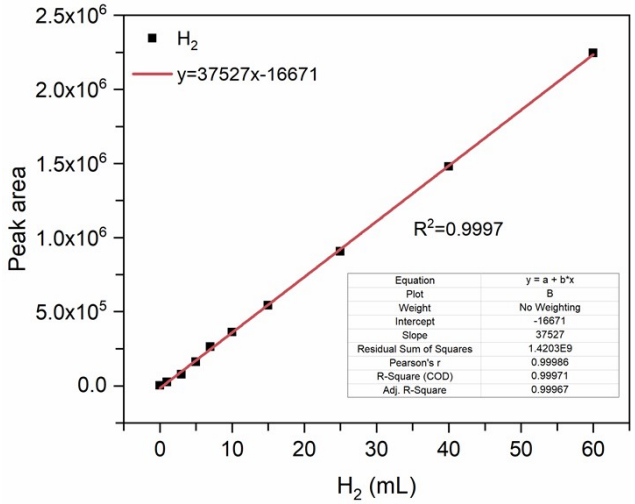

Fig. S20 The standard curve of H_2 by GC (nitrogen as carrier gas) equipped with FID.

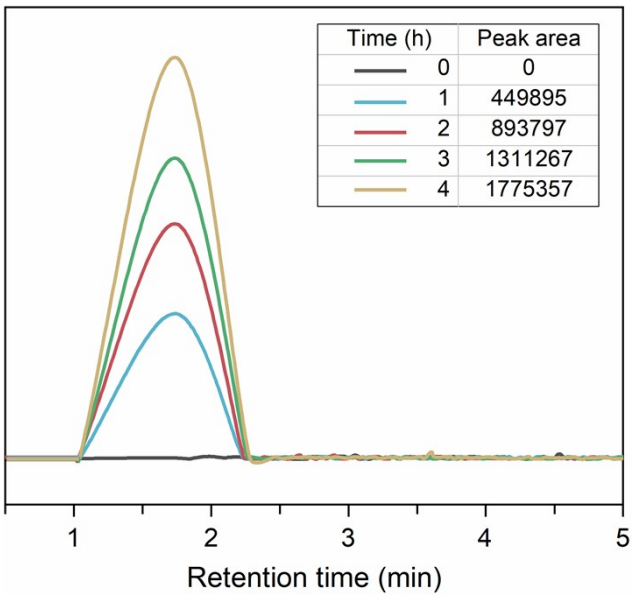

Fig. S21 GC spectrum of H_2 under different reaction times.

Table S1 Elemental analysis of PSO and PSO@NiFeLDH-15.

Sample	Theoretical data				Experimental data			
	C(%)	O(%)	S(%)	H(%)	C(%)	O(%)	S(%)	H(%)
PSO	67.21	14.94	14.94	2.80	58.40	14.51	12.64	2.72
PSO@NiFeLDH-15	57.13	18.09	12.69	2.72	53.69	21.76	10.88	2.48

Table S2 The ICP-MS analysis for NiFeLDH and PSO@NiFeLDH composites.

Sample	Experimental data		Ni/Fe
	Ni (%)	Fe (%)	
NiFeLDH	40.12	5.59	7.17
PSO@NiFeLDH-5	1.22	0.23	5.30
PSO@NiFeLDH-10	3.18	0.47	6.76
PSO@NiFeLDH-15	4.09	0.61	6.70
PSO@NiFeLDH-25	4.67	0.68	6.86
PSO@NiFeLDH-50	17.4	2.51	6.93

Table S3 The surface properties of NiFeLDH, PSO and PSO@NiFeLDH.

Sample	S_{BET} (m^2 g^{-1})	Average pore volume (cm^3 g^{-1})
NiFeLDH	98.07	0.161
PSO	12.22	0.133
PSO@NiFeLDH-5	14.20	0.156
PSO@NiFeLDH-10	16.38	0.132
PSO@NiFeLDH-15	46.58	0.224
PSO@NiFeLDH-25	38.04	0.182
PSO@NiFeLDH-50	18.19	0.164

Table S4 Optical and electrochemical properties of NiFeLDH and PSO.

Sample	Reduction potential (eV)	Oxidation potential (eV)	E_{LUMO}(VB) (eV)	E_{HOMO}(CB) (eV)	E_g^a (eV)
NiFeLDH	−0.61	1.59	−3.90	−6.10	2.20
PSO	−1.13	1.43	−3.38	−5.94	2.56

$E_{HOMO(CB)} = -e(E_{ox} + 4.8 - E_{1/2}^{(Fc/Fc+)})$ (eV) and $E_{LUMO(VB)} = -e(E_{re} + 4.8 - E_{1/2}^{(Fc/Fc+)})$ (eV) respectively, where E_{re} and E_{ox} are the onset of the reduction and oxidation potential vs the SCE. $E_{1/2}^{(Fc/Fc+)} = 0.29$ V vs SCE, $E_g^a = E_{LUMO} - E_{HOMO}$.

Table S5 Summary of reported heterojunction photocatalysts for hydrogen evolution rates.

Catalyst	Co-catalyst	Sacrificial agent	Illumination	HER (mmol h^{-1} g^{-1})	Ref
PSO@NiFeLDH	-	TEOA	>420 nm (Xe, 300 W)	52.80	This work
WO_3@TpPa-1-COF/rGO	Pt	ascorbic acid	>420 nm	26.73	S1

			(Xe, 300 W)		
Cd/Ni-MOFs	-	lactic acid	>420 nm (Xe, 300 W)	42.76	S2
CdS–NiPc	-	lactic acid	>420 nm (Xe, 300 W)	17.74	S3
$CZ_{0.5}S$@50ZS-3N/8CN	Ni_2P/g-C_3N_4	Na_2S/Na_2SO_3	>420 nm (Xe, 300 W)	55.43	S4
PDBTSO/TiO_2	Pt	TEOA	>420 nm (Xe, 300 W)	51.50	S5
CNS–COF	Pt	TEOA	>420 nm (Xe, 300 W)	46.40	S6
$Zn_{0.5}Cd_{0.5}S$/ZIF-67	-	lactic acid	>420 nm (Xe, 300 W)	23.26	S7
ZIF2@CdS100	-	lactic acid	>420 nm (Xe, 300 W)	17.19	S8
Flu-DFBZ/g-C_3N_4	Pt	TEOA	>420 nm (Xe, 300 W)	14.85	S9
$Zn_xCd_{1-x}S$	-	Na_2S/Na_2SO_3	>420 nm (Xe, 300 W)	13.46	S10
CdS-CTF-1	Pt	lactic acid	>420 nm (Xe, 300 W)	11.43	S11
TiO_2-TpPa-1-COF	Pt	ascorbic acid	>420 nm (Xe, 300 W)	11.19	S12
NH_2-MIL-125(Ti)/ZnCr-LDH	Pt	TEOA	>420 nm (Xe, 300 W)	127.60	S13
WO_{3-X}/Ag/ZnCrLDH	-	CH_3OH	>420 nm (Xe, 150 W)	29.37	S14
Ni_2P/Ni@C/g-C_3N_4-550	-	TEOA	>420 nm (Xe, 300 W)	18.40	S15

$NiS/Zn_{0.5}Cd_{0.5}S$	-	Na_2S/Na_2SO_3	>420 nm (Xe, 300 W)	16.78	S16
$Zn_{0.5}Cd_{0.5}S/ZnO/Zn_{0.5}Cd_{0.5}$	-	Na_2S/Na_2SO_3	>420 nm (Xe, 300 W)	28.60	S17
BE–Au–TiO_2	Au	TEOA	>420 nm (Xe, 300 W)	26.04	S18
NH_2-UiO-66/TpPa-1-COF	Pt	ascorbic acid	>420 nm (Xe, 300 W)	23.41	S19
α-Fe_2O_3/g-C_3N_4	Pt	TEOA	>420 nm (Xe, 300 W)	31.40	S20
Co-Doped $Zn_{0.5}Cd_{0.5}S$	-	Na_2S/Na_2SO_3	>420 nm (Xe, 300 W)	17.36	S21

Table S6 ICP-MS for PSO@NiFeLDH-15 and reused PSO@NiFeLDH-15 after reaction.

Sample	Ni (%)	Fe (%)
PSO@NiFeLDH-15	4.09	0.61
Reused PSO@NiFeLDH-15	3.45	0.51

Table S7 Fitted decay time of PSO and PSO@NiFeLDH-15.

Sample	τ_1 (ns)	Rel (%)	τ_2 (ns)	Rel (%)	τ (ns)
PSO	0.704	56.75	3.188	43.25	1.321
PSO@NiFeLDH-15	0.781	49.14	3.778	50.86	1.742

References:

S1. H. Yan, Y. H. Liu, Y. Yang, H. Y. Zhang, X. R. Liu, J. Z. Wei, L. L. Bai, Y. Wang and F. M. Zhang, *Chem. Eng. J.*, 2022, **431**, 133404.

S2. C. F. Liu, Y. Y. Liu, Z. H. Xiang, D. H. Liu and Q. Y. Yang, *Ind. Eng. Chem. Res*., 2021, **60**, 11439–11449.

S3. J. L. Sheng, C. Q. Wang, F. Duan, S. R. Yan, S. L. Lu, H. Zhu, M. L. Du, X. Chen and M. Q. Chen, *Catal. Sci. Technol.*, 2021, **11**, 7683–7693.

S4. X. W. Ma, Q. Q. Ruan, J. K. Wu, Y. Zuo, X. P. Pu, H. F. Lin, X. J. Yi, Y. Y. Li and L. Wang, *Dalton Trans*., 2020, **49**, 6259–6269.

S5. G. Shu, Y. Wang, Y. D. Li, S. Zhang, J. X. Jiang and F. Wang, *J. Mater. Chem. A*, 2020, **8**, 18292–18301.

S6. M. L. Luo, Q. Yang, W. B. Yang, J. H. Wang, F. F. He, K. W. Liu, H. M. Cao and H. J. Yan, *Small*, 2020, **16**, 2001100.

S7. H. M. Gong, X. J. Zhang, G. R. Wang, Y. Liu, Y. B. Li and Z. L. Jin, *Mol. Catal*., 2020, **485**, 110832.

S8. Z. B. Yu, L. Qian, T. Zhong, Q. Ran, J. Huang, Y. P. Hou, F. Y. Li, M. J. Li, Q. Q. Sun and H. Q. Zhang, *Mol. Catal*., 2020, **485**, 110797.

S9. H. N. Ye, Z. Q. Wang, F. T. Yu, S. C. Zhang, K. Y. Kong, X. Q. Gong, J. L. Hua and H. Tian, *Appl. Catal., B*, 2020, **267**, 118577.

S10. K. Q. Li, H. L. Xiong, X. Wang, Y. L. Ma, T. N. Gao, Z. L. Liu, Y. L. Liu, M. H. Fan, L. Zhang and Z. A. Qiao, *Inorg. Chem*., 2020, **59**, 5063–5071.

S11. D. Wang, H. Zeng, X. Xiong, M. F. Wu, M. Xia, M. Xie, J. P. Zou and S. L. Luo, *Sci. Bull*., 2020, **65**, 113–122.

S12. C. C. Li, M. Y. Gao, X. J. Sun, H. L. Tang, H. Dong and F. M. Zhang, *Appl. Catal., B*, 2020, **266**, 118586.

S13. M. Sohail, H. Kim and T. W. Kim, *Sci. Rep*., 2019, **9**, 7584.

S14. D. P. Sahoo, S. Patnaik and K. Parida, *ACS Omega*, 2019, **4**, 14721–14741.

S15. J. X. Xu, Y. H. Qi and L. Wang, *Appl. Catal., B*, 2019, **246**, 72–81.

S16. X. X. Zhao, J. R. Feng, J. Liu, W. Shi, G. M. Yang, G. C. Wang and P. Cheng, *Angew. Chem., Int. Ed*., 2018, **130**, 9938–9942.

S17. J. M. Chen, Z. R. Shen, S. M. Lv, K. Shen, R. F. Wu, X. F. Jiang, T. Fan, J. Y. Chen and Y. W. Li, *J. Mater. Chem. A*, 2018, **6**, 19631–19642.

S18. J. Xiao, Y. Z. Luo, Z. X. Yang, Y. G. Xiang, X. H. Zhang and H. Chen, *Catal. Sci. Technol.*,

2018, **8**, 2477–2487.

S19. F. M. Zhang, J. L. Sheng, Z. D. Yang, X. J. Sun, H. L. Tang, M. Lu, H. Dong, F. C. Shen, J. Liu and Y. Q. Lan, *Angew. Chem., Int. Ed*., 2018, **57**, 12106–12110.

S20. X. J. She, J. J. Wu, H. Xu, J. Zhong, Y. Wang, Y. H. Song, K. Q. Nie, Y. Liu, Y. C. Yang and M. T. F. Rodrigues, *Adv. Energy Mater*., 2017, **7**, 1700025.

S21. X. Tang, J. H. Zhao, Y. H. Li, Z. J. Zhou, K. Li, F. T. Liu and Y. Q. Lan, *Dalton Trans*., 2017, **46**, 10553–10557.